ISSN 1674-1056
http://cpb.iphy.ac.cn
http://iopscience.iop.org/cpb
中国物理 B
Chinese Physics
中国物理
Chinese Physics B

Impact of the spatial coherence on self-interference digital holography

Xingbing Chao(潮兴兵), Yuan Gao(高源), Jianping Ding(丁剑平), and Hui-Tian Wang(王慧田)
Citation: Chin. Phys. B, 2021, 30 (**8**): 084212. DOI: 10.1088/1674-1056/abd766
Journal homepage: http://cpb.iphy.ac.cn; http://iopscience.iop.org/cpb

What follows is a list of articles you may be interested in

Incoherent digital holographic spectral imaging with high accuracy of image pixel registration

Feng-Ying Ma(马凤英), Xi Wang(王茜), Yuan-Zhuang Bu(卜远壮), Yong-Zhi Tian(田勇志), Yanli Du(杜艳丽) , Qiao-Xia Gong(弓巧侠), Ceyun Zhuang(庄策云), Jinhai Li(李金海), and Lei Li(李磊)
Chin. Phys. B, 2021, 30 (**4**): 044202. DOI: 10.1088/1674-1056/abd2aa

Two-step phase-shifting Fresnel incoherent correlation holography based on discrete wavelet transform

Meng-Ting Wu(武梦婷), Yu Zhang(张雨), Ming-Yu Tang(汤明玉), Zhi-Yong Duan(段智勇), Feng-Ying Ma(马凤英), Yan-Li Du(杜艳丽), Er-Jun Liang(梁二军), and Qiao-Xia Gong(弓巧侠)
Chin. Phys. B, 2020, 29 (**12**): 124201. DOI: 10.1088/1674-1056/abab7d

Single-shot phase-shifting digital holography with a photon-sieve-filtering telescope

You Li(李优), Yao-Cun Li(李垚村), Jun-Yong Zhang(张军勇), Yan-Li Zhang(张艳丽), Xue-Mei Li(李雪梅)
Chin. Phys. B, 2019, 28 (**8**): 084205. DOI: 10.1088/1674-1056/28/8/084205

Speckle reduction by selective spatial-domain mask in digital holography

Ming-Da Liang(梁明大), Li Chen(陈丽), Yi-Hua Hu(胡义华), Wei-Tao Lin(林伟涛), Yong-Hao Chen(陈永昊)
Chin. Phys. B, 2018, 27 (**10**): 104202. DOI: 10.1088/1674-1056/27/10/104202

Optical encryption of multiple three-dimensional objects based on multiple interferences and single-pixel digital holography

Ying Wang(王莹), Qi Liu(刘琦), Jun Wang(王君), Qiong-Hua Wang(王琼华)
Chin. Phys. B, 2018, 27 (**3**): 034202. DOI: 10.1088/1674-1056/27/3/034202

SPECIAL TOPIC — Optical field manipulation

Impact of the spatial coherence on self-interference digital holography*

Xingbing Chao(潮兴兵)[1,4], Yuan Gao(高源)[1], Jianping Ding(丁剑平)[1,2,3,†], and Hui-Tian Wang(王慧田)[1,2]

[1] National Laboratory of Solid State Microstructures and School of Physics, Nanjing University, Nanjing 210093, China
[2] Collaborative Innovation Center of Advanced Microstructures, Nanjing University, Nanjing 210093, China
[3] Collaborative Innovation Center of Solid-State Lighting and Energy-Saving Electronics, Nanjing University, Nanjing 210093, China
[4] College of Science, Jiujiang University, Jiujiang 332005, China

(Received 30 October 2020; revised manuscript received 16 December 2020; accepted manuscript online 30 December 2020)

Owing to the unique feature that the signal and reference waves of self-interference digital holography (SIDH) contain the same spatial information from the same point of object, compared with conventional digital holography, the SIDH has the special spatial coherence properties. We present a statistical optics approach to analyzing the formation of cross-correlation image in SIDH. Our study reveals that the spatial coherence of illumination light can greatly influence the imaging characteristics of SIDH, and the impact extent of the spatial coherence depends substantially on the recording distance of hologram. The theoretical conclusions are supported well by numerical simulation and optical experiments.

Keywords: holography, imaging and optical processing, photon statistics and coherence theory, interference

PACS: 42.40.–i, 42.30.–d, 42.25.Hz **DOI:** 10.1088/1674-1056/abd766

1. Introduction

Digital holography (DH) is receiving extensive interest not only due to the everlasting quest to quantitatively characterize complex three-dimensional (3D) light field, but also owing to the state of the art advances in digital technology, which enables the high-sensitive and high-resolution recording as well as the fast digital reconstruction of hologram.[1–4] However, in conventional digital holography, since the reference wave is required to interfere with the object wave, the coherent illumination is essential, which hinders the full explorations and applications of digital holography. The coherent illumination excludes the use of ordinary light sources, and can incur speckle and parasitic interference noise in the holographic recording and reconstructing process. In order to break the coherence barrier and expand its applications, the digital holographic schemes allowing low coherent source have been studied. In recent years, many research groups began to pay renewed attention to the incoherent digital holography. Among various schemes, a kind of techniques referred to as the self-interference digital holography (SIDH)[5–7] is particularly attractive and has been used in various applications, such as color holography,[8] fluorescence microscopy,[9] 3D imaging,[10] super-resolution,[11,12] adaptive optics,[13,14] imaging through random media,[15,16] and others.[17–20]

The optical trick of SIDH is that, with the aid of suitable optical components, the incident wave originated from an object point is split into two parts, and then they can be recombined together in a recording plane and interfere with each other to form a hologram. Even though extensive works on SIDH have been carried out, some essential issues of SIDH remain to be clarified. One of the most concerned issues is the quality of the image reconstructed from an SIDH, and hence many approaches[12,21,22] have devoted to analyzing and improving the resolution of SIDH. As is well known, there are many factors that influence the resolution of imaging system. As a digital holography, SIDH suffers from some drawbacks inherent to electronic devices, such as the aperture effect[21,22] and limited number and size of pixel[23] in devices which can detract from the imaging resolution of digital holography. Furthermore, to deepen the understanding of the quantitative relationship between an object and its image, it is essential for us to know the coherence properties of optical field, because the optical coherence has potential influences on the quality of the reconstructed image that is ultimately observed.[24,25]

Due to spatially incoherent illumination, the image quality of SIDH is superior to that of conventional holography in sense of its inherently speckle-free property. However, the spatially incoherent light is an ideal and extreme case, and any natural light is correlated over distances that are at least of the order of the mean wavelength of the light.[26] In short, a light is more or less partially spatially coherent. Hence, the spatial coherence effects cannot be completely neglected in holographic imaging systems especially for an SIDH, which is different from the conventional digital holography in the as-

*Project supported by the National Natural Science Foundation of China (Grant Nos. 91750202, 91750114, and 11922406), the National Key Research and Development Program of China (Grant Nos. 2018YFA0306200 and 2017YFA0303700), and the Science and Technology Project of Jiangxi Provincial Education Department, China (Grant No. GJJ190915).

†Corresponding author. E-mail: jpding@nju.edu.cn

© 2021 Chinese Physical Society and IOP Publishing Ltd

pect that both the signal wave and reference wave of SIDH originate from the same point of object. To date, however, the reports of the impact of spatial coherence on SIDH are scarce.

In this paper, we have presented a statistical optics approach to analyzing the formation of cross-correlation images in SIDH. Our study reveals that the spatial coherence of illumination light can greatly influence the imaging characteristics of SIDH, and the impact extent of the spatial coherence depends substantially on the recording distance of hologram. The theoretical conclusions are supported well by numerical and optical experiments.

2. Spatial coherence properties of SIDH

The conceptual construction of a typical SIDH with common-path and in-line configuration is schematically depicted in Fig. 1, which outlines both the optically implemented recording process and digitally accomplished reconstruction process via a computer. In the recording process, an object wave, after passing the collimating lens, illuminates a spatial light modulator (SLM) that carries a quadratic-phase holographic function resembling diffractive lens. Assuming that the holographic function of SLM to be $t(x_{\rm s},y_{\rm s}) = a + b\exp\left[-{\rm i}\pi(x_{\rm s}^2+y_{\rm s}^2)/(\lambda f_{\rm d}) + {\rm i}\theta_j\right]$, where a and b are the constant, λ is the wavelength, $f_{\rm d}$ is the focal length of the diffractive lens, and θ_j is a phase shift at the j-th step,[27] the SLM can divide the incident wave into two waves, which serve as the signal and reference waves, respectively. The two waves produce an interference pattern in the sensor area of a CCD camera, thus forming a digital hologram. Since the signal and reference waves actually originate from the same point in the object plane, the two waves can mutually interfere with each other (*i.e.*, self-interference) even though the object is under spatially incoherent illumination. From the acquired hologram, the reconstructed image is calculated by a computer, which simulates the optical reconstruction procedure.

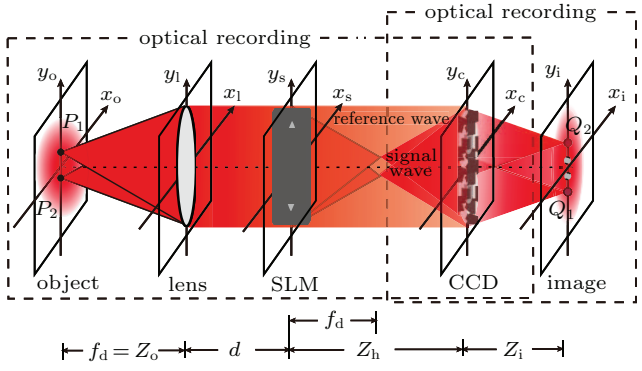


Fig. 1. Schematic diagram of SIDH with common-path configuration.

Let us start from two arbitrary points $\boldsymbol{P}_1(x_{P_1},y_{P_1})$ and $\boldsymbol{P}_2(x_{P_2},y_{P_2})$ in the object plane ($Z_0 = f_0$). To simplify discussion, we assume that the aperture of the collimating lens is so large enough that the vignetting effects may be neglected. After the collimating lens, the light from the m-th ($m = 1,2$) object point at $\boldsymbol{P}_m(x_{P_m},y_{P_m})$ becomes a plane wave impinging the SLM at (x_s,y_s), as expressed by

$$U^-(\boldsymbol{S}) = U(\boldsymbol{P}_m)\exp\left[-\frac{{\rm i}2\pi}{\lambda f_0}(x_{P_m}x_s + y_{P_m}y_s)\right], \tag{1}$$

where $U(\boldsymbol{P}_m)$ is the complex amplitude at $\boldsymbol{P}_m$, $U(\boldsymbol{P}_m) = u(\boldsymbol{P}_m)\exp[{\rm i}\varphi(\boldsymbol{P}_m)]$. After being imparted to the incident wave, the two terms in the holographic function of the SLM lead to two waves: the unmodulated one called the reference wave, $U_{R_m}(\boldsymbol{S}) = aU^-(\boldsymbol{S})$, and the modulated one called the signal wave, $U^j_{O_m}(\boldsymbol{S}) = bU^-(\boldsymbol{S})\exp[-{\rm i}\pi(x_s^2+y_s^2)/\lambda f_{\rm d} + {\rm i}\theta_j]$. After propagating over a distance $Z_{\rm h}$ on to the recording plane, the complex amplitudes of the reference and signal waves at (x_c,y_c) on the CCD can be expressed by

$$\begin{aligned} &U_{R_m}(\boldsymbol{C}) \\ &= AP_{\rm C}(\boldsymbol{C})\iint P_{\rm S}(\boldsymbol{S})U_{R_m}(\boldsymbol{S}) \\ &\quad\times\exp\left\{\frac{{\rm i}\pi}{\lambda Z_{\rm h}}\left[(x_s-x_c)^2+(y_s-y_c)^2\right]\right\}{\rm d}x_s{\rm d}y_s, \end{aligned} \tag{2}$$

$$\begin{aligned} &U^j_{O_m}(\boldsymbol{C},\theta_j) \\ &= BP_{\rm C}(\boldsymbol{C})\iint P_{\rm S}(\boldsymbol{S})U_{O_m}(\boldsymbol{S}) \\ &\quad\times\exp\left\{\frac{{\rm i}\pi}{\lambda Z_{\rm h}}[(x_s-x_c)^2+(y_s-y_c)^2]\right\}{\rm d}x_s{\rm d}y_s, \end{aligned} \tag{3}$$

with $P_{\rm C}(\boldsymbol{C})$ and $P_{\rm S}(\boldsymbol{S})$ denoting the pupil function of the CCD and the SLM, respectively, and A and B are constant factors. According to the self-interference principle, a complex amplitude of the total field at arbitrary point (x_c,y_c) can be expressed by

$$U^j(\boldsymbol{C}) = U_{O_1}(\boldsymbol{C},\theta_j) + U_{R_1}(\boldsymbol{C}) + U_{O_2}(\boldsymbol{C},\theta_j) + U_{R_2}(\boldsymbol{C}). \tag{4}$$

Hence, the intensity to be recorded by the CCD is

$$\begin{aligned} I^j(C) &= \left\langle U^j(\boldsymbol{C})U^{j*}(\boldsymbol{C})\right\rangle \\ &= \sum_{m=1}^{2}\sum_{m'=1}^{2}\left\langle U_{R_m}(\boldsymbol{C})U^*_{R_{m'}}(\boldsymbol{C})\right\rangle \\ &\quad+\sum_{m=1}^{2}\sum_{m'=1}^{2}\left\langle U_{O_m}(\boldsymbol{C},\theta_j)U^*_{O_{m'}}(\boldsymbol{C},\theta_j)\right\rangle \\ &\quad+\sum_{m=1}^{2}\sum_{m'=1}^{2}\left\langle U_{R_m}(\boldsymbol{C})U^*_{O_{m'}}(\boldsymbol{C},\theta_j)\right\rangle \\ &\quad+\sum_{m=1}^{2}\sum_{m'=1}^{2}\left\langle U_{O_m}(\boldsymbol{C},\theta_j)U^*_{R_{m'}}(\boldsymbol{C})\right\rangle, \end{aligned} \tag{5}$$

where the asterisk denotes the complex conjugate, and the angular brackets represent the ensemble averaging. Of interest in Eq. (5) is the fourth term, which will be used to reconstruct the object point in the successive digital reconstruction process, and is expressed in the more explicit form

$$t(\boldsymbol{C}) = \left\langle U_{O_1}(\boldsymbol{C})U^*_{R_1}(\boldsymbol{C})\right\rangle + \left\langle U_{O_2}(\boldsymbol{C})U^*_{R_2}(\boldsymbol{C})\right\rangle$$

$$+\left\langle U_{O_1}(\boldsymbol{C})U^*_{R_2}(\boldsymbol{C})\right\rangle+\left\langle U_{O_2}(\boldsymbol{C})U^*_{R_1}(\boldsymbol{C})\right\rangle. \quad (6)$$

This term can be extracted from the three holograms recorded sequentially through three-step phase shifting with $\theta_1=0$, $\theta_2=2\pi/3$, and $\theta_3=4\pi/3$.[28] The first two terms of Eq. (6) are the cross correlation between the signal and reference waves originated from the same object point $\boldsymbol{P}_m$ ($m=1$ or 2), which are mutually coherent regardless of the spatial coherence of the light source, and thus can be expressed in terms of coherent fields, $\left\langle U_{O_m}(\boldsymbol{C})U^*_{R_m}(\boldsymbol{C})\right\rangle = U_{O_m}(\boldsymbol{C})U^*_{R_m}(\boldsymbol{C})$. After some derivations this cross correlation turns out to be

$$U_{O_m}(\boldsymbol{C})U^*_{R_m}(\boldsymbol{C}) = u^2(\boldsymbol{P}_m)\exp\left\{\frac{-\mathrm{i}k}{2(f_\mathrm{d}-Z_\mathrm{h})}\left[\left(x_\mathrm{C}+\frac{Z_\mathrm{h}}{f_0}x_{P_m}\right)^2+\left(y_\mathrm{C}+\frac{Z_\mathrm{h}}{f_0}y_{P_m}\right)^2\right]\right\}, \quad (7)$$

wherein some inessential factors independent of coordinates of (x_P,y_P) and $(x_\mathrm{C},y_\mathrm{C})$ are omitted for brevity. Note that the quadratic phase factor in Eq. (7) represents a spherical wave convergent at a point locating at the distance $f_\mathrm{d}-Z_\mathrm{h}$ (*i.e.*, the reconstruction distance) away from the CCD plane. The reconstruction is digitally implemented by calculating the Fresnel diffraction integral of Eq. (7). After some derivations with the aid of the method of stationary phase (given in the Appendix A), the reconstructed field from the self-interference terms of the hologram is obtained as the integral over all the responses of the object points, as follows:

$$\begin{aligned}U_{O_mR_m}(\boldsymbol{Q}) &= \iint\!\!\iint U_{O_m}(\boldsymbol{C})U^*_{R_m}(\boldsymbol{C})\exp\left\{\frac{\mathrm{i}k\left[(x_\mathrm{C}-x_Q)^2+(y_\mathrm{C}-y_Q)^2\right]}{2(f_\mathrm{d}-Z_\mathrm{h})}\right\}\mathrm{d}x_\mathrm{C}\,\mathrm{d}y_\mathrm{C}\,\mathrm{d}x_{P_m}\,\mathrm{d}y_{P_m}\\ &= M_{O_mR_m}\iint\exp\left[\frac{\mathrm{i}k(x_Q^2+y_Q^2)}{2(f_\mathrm{d}-Z_\mathrm{h})}\right]\delta\left[x_Q+\frac{Z_\mathrm{h}}{f_0}x_{P_m}\right]\delta\left[y_Q+\frac{Z_\mathrm{h}}{f_0}y_{P_m}\right]\mathrm{d}x_{P_m}\,\mathrm{d}y_{P_m}, \quad (8)\end{aligned}$$

where $M_{O_mR_m}$ is a multiplying factor independent of the coordinates (x_P,y_P).

The last two terms in Eq. (6) are of the mutual intensity representing the mutual interference between the signal and reference waves originated from different object points; the contributions of these mutual intensities increase with the increase of spatial coherence of optical field. Taking into account the propagation of partially coherent field,[29] the mutual intensity in the resulting hologram turns out to be

$$\begin{aligned}&\left\langle U_{O_m}(\boldsymbol{C})U^*_{R_{m'}}(\boldsymbol{C})\right\rangle\\ &= \left\langle u(\boldsymbol{P}_m)u(\boldsymbol{P}_{m'})\exp\left[\mathrm{i}\varphi(\boldsymbol{P}_m)-\mathrm{i}\varphi(\boldsymbol{P}_{m'})\right]\right\rangle\\ &\quad\times\exp\left[\mathrm{i}\varphi_{O_m}(\boldsymbol{C})-\mathrm{i}\varphi_{R_{m'}}(\boldsymbol{C})\right], \quad (9)\end{aligned}$$

where $m=1,2$, $m'=1,2$, and $m\neq m'$. Under a partially coherent light illumination with Gaussian–Schell model (GSM) correlation,[24] the mutual intensity in the observation plane becomes

$$\begin{aligned}&\left\langle u(\boldsymbol{P}_m)u(\boldsymbol{P}_{m'})\exp\left[\mathrm{i}\varphi(\boldsymbol{P}_m)-\mathrm{i}\varphi(\boldsymbol{P}_{m'})\right]\right\rangle\\ &= \exp\left[-\frac{|\boldsymbol{P}_m-\boldsymbol{P}_{m'}|^2}{2\sigma^2}\right]\exp\left[-\frac{(\boldsymbol{P}_m^2+\boldsymbol{P}_{m'}^2)}{4\rho^2}\right], \quad (10)\end{aligned}$$

where ρ and σ are the widths of the transverse intensity profile and of the degree of coherence, respectively. By substituting Eq. (10) into Eq. (9), and following the calculation method used in Eq. (8), we can get the reconstructed field from the mutual-interference terms of the hologram as follows:

$$\begin{aligned}&\left\langle U_{O_m}(\boldsymbol{Q})U^*_{R_{m'}}(\boldsymbol{Q})\right\rangle\\ &= \exp\left[\frac{\mathrm{i}k(x_Q^2+y_Q^2)}{2(f_\mathrm{d}-Z_\mathrm{h})}\right]M'_{O_m,R_{m'}}\\ &\quad\times\iint\!\!\iint\exp\left[-\frac{|\boldsymbol{P}_m-\boldsymbol{P}_{m'}|^2}{2\sigma^2}\right]\exp\left[-\frac{(\boldsymbol{P}_m^2+\boldsymbol{P}_{m'}^2)}{4\rho^2}\right]\\ &\quad\times\delta\left[x_Q+\frac{f_\mathrm{d}}{f_0}x_{P_m}+\frac{(Z_\mathrm{h}-f_\mathrm{d})}{f_0}x_{P_{m'}}\right]\\ &\quad\times\delta\left[y_Q+\frac{f_\mathrm{d}}{f_0}y_{P_m}+\frac{(Z_\mathrm{h}-f_\mathrm{d})}{f_0}y_{P_{m'}}\right]\mathrm{d}x_{P_{m'}}\,\mathrm{d}y_{P_{m'}}\,\mathrm{d}x_{P_m}\,\mathrm{d}y_{P_m}, \quad (11)\end{aligned}$$

where $M'_{O_m,R_{m'}}$ is a multiplying factor independent of the coordinates (x_P,y_P). Taking into account the properties of δ function in Eqs. (8) and (11), we can get the transverse coordinates of the images in the following relation:

$$\begin{cases}\boldsymbol{Q}_1: x_{Q_1}=-\dfrac{Z_\mathrm{h}}{f_0}x_{P_1},\quad y_{Q_1}=-\dfrac{Z_\mathrm{h}}{f_0}y_{P_1};\\ \boldsymbol{Q}_2: x_{Q_2}=-\dfrac{Z_\mathrm{h}}{f_0}x_{P_2},\quad y_{Q_2}=-\dfrac{Z_\mathrm{h}}{f_0}y_{P_2};\\ \boldsymbol{Q}_3: x_{Q_3}=-\dfrac{f_\mathrm{d}}{f_0}x_{P_1}+\dfrac{f_\mathrm{d}-Z_\mathrm{h}}{f_0}x_{P_2},\\ \qquad y_{Q_3}=-\dfrac{f_\mathrm{d}}{f_0}y_{P_1}+\dfrac{f_\mathrm{d}-Z_\mathrm{h}}{f_0}y_{P_2};\\ \boldsymbol{Q}_4: x_{Q_4}=-\dfrac{f_\mathrm{d}}{f_0}x_{P_2}+\dfrac{f_\mathrm{d}-Z_\mathrm{h}}{f_0}x_{P_1},\\ \qquad y_{Q_4}=-\dfrac{f_\mathrm{d}}{f_0}y_{P_2}+\dfrac{f_\mathrm{d}-Z_\mathrm{h}}{f_0}y_{P_1}.\end{cases} \quad (12)$$

From Eq. (12), we can find that under the condition of partially coherent illumination, there are four image spots in the reconstructed image plane. Image spots at $\boldsymbol{Q}_1$ and $\boldsymbol{Q}_2$ are called the self-interference reconstructed image (SIRI) since they result from the self-interference term in the holographic function expressed in Eq. (6); and the SIRI at $\boldsymbol{Q}_1$ and $\boldsymbol{Q}_2$ are what the SIDH should reconstruct with respect to the single object point $\boldsymbol{P}_1$ and $\boldsymbol{P}_2$, respectively. Reconstructed spots at

$\boldsymbol{Q}_3$ and $\boldsymbol{Q}_4$ are called the mutual-interference reconstructed image (MIRI). In other words, the quality of images reconstructed from the SIDH will deteriorate as the spatial coherence of illumination light increases; and the best quality SIRI can be obtained under a spatially incoherent illumination since its statistical correlation between different object points tends to zero.

It is worth to note that in Eq. (11) the position and number of MIRIs depend on the recording distance $Z_{\rm h}$ between SLM and CCD. As $Z_{\rm h}=0$, two SIRIs overlap with each other to form one SIRI, and there are two MIRIs appearing in the image plane. As $Z_{\rm h}=f_{\rm d}$, there are only two SIRIs, but MIRIs vanish. For the case of $Z_{\rm h}=2f_{\rm d}$, two MIRIs are overlapped with each other to form one MIRI, and there are three image spots in total. If $Z_{\rm h}<f_{\rm d}$, the two MIRIs symmetrically locate outside the two SIRIs; however, if $Z_{\rm h}>f_{\rm d}$, the two MIRIs symmetrically locate inside the two SIRIs. In the following numerical simulations and optical experiments, we shall demonstrate the validity of our theoretical analysis.

3. Numerical simulations and optical experiments

3.1. Simulation investigation into the impact of spatial coherence

According to the optical coherence theory, the statistical relationships between the complex amplitudes of different points in the object plane can affect the statistical relationships between the corresponding impulse responses in the recording plane in Fig. 1. Thus, given N object points in the object plane, we have in the sensor area of CCD camera the complex amplitude $U_m(\boldsymbol{C},\theta_j)=U_{O_m}(\boldsymbol{C},\theta_j)+U_{R_m}(\boldsymbol{C})$ $(m=1,2,\ldots,N)$ resulting from the m-th object point after the SLM modulation, and the recorded intensity (hologram) for the j-th phase shift becomes

$$I_j(\boldsymbol{C},\theta_j)=\left\langle\left|\sum_{m=1}^{N}U_m(\boldsymbol{C},\theta_j)\right|^2\right\rangle=\sum_{m=1}^{N}\left\langle\left|U_m(\boldsymbol{C},\theta_j)\right|^2\right\rangle+\sum_{m=1}^{N}\sum_{n=1}^{N}\left\langle U_m(\boldsymbol{C},\theta_j)U_n^*(\boldsymbol{C},\theta_j)\right\rangle,\ (m\neq n).\quad(13)$$

The hologram consists of two terms: the first term represents the single-point intensity, and the second term represents the cross-correlation between any two object points and can also be defined by

$$\sum_{m=1}^{N}\sum_{m'=1}^{N}\left\langle U_m(\boldsymbol{C},\theta_j)U_{m'}^*(\boldsymbol{C},\theta_j)\right\rangle=\sum_{m=1}^{N}\sum_{m'=1}^{N}\left\langle U_m(\boldsymbol{C},\theta_j)\right\rangle\left\langle U_{m'}^*(\boldsymbol{C},\theta_j)\right\rangle\mu(\boldsymbol{C},\boldsymbol{C}'),\ (m\neq m'),\quad(14)$$

where $\mu(\boldsymbol{C},\boldsymbol{C}')$ is the modulus of the complex coherence degree. For the illumination of fully coherent (or incoherent) light, $\mu(\boldsymbol{C},\boldsymbol{C}')$ is equal to 1 (or 0). For a partially coherent light, we have $\mu(\boldsymbol{C},\boldsymbol{C}')=\exp\left[-|\boldsymbol{C}-\boldsymbol{C}'|^2/2\sigma^2\right]$ in the sense of GSM and the spatial correlation degree of the optical field can be changed by adjusting the coherence-width parameter σ.

In this paper, with the aid of Matlab (R2013a) software, we use the computer (DELL, CPU e5-2650, RAM: 128 GB) to simulate an optical experiment as schematically illustrated in Fig. 1. The simulation parameters are set such that they reflect practical arrangements used in the following optical experiments. A 2048×2048 array with 8.0-μm sampling pitch is chosen as an object plane which is placed at the front focal plane of the lens ($R_1=12.5$ mm, $f_0=0.12$ m), and illuminated by a plane wave ($\lambda=632.8$ nm). The distance $Z_{\rm h}$ between SLM (with a aperture size $R_{\rm s}=4.32$ mm and a pixel pitch 8.0 μm) and CCD (a aperture size $R_{\rm c}=3.54$ mm and a pixel pitch 3.45 μm) varies from 0 m to 0.60 m with a 0.05-m increment. Other parameters include $d=0.20$ m and $f_{\rm d}=0.30$ m. An adaptive computational algorithm[30] is used for simulating optical recording and digital reconstructing processes. This algorithm, based on scalar diffraction theory and fast Fourier transform, is suitable for different diffraction regimes and arbitrary sampling rates. In the following numerical investigations, we consider the two cases: double-point object and multi-point object, respectively, which are illuminated by a fully incoherent light (FIL), a fully coherent light (FCL) and a partially coherent light (PCL), respectively. For the PCL, we choose σ to be 80.0, 160.0, and 320 μm, respectively, in the recording plane of hologram.

For the case of double-point object, the spacing of two object points is set to be 320.0 μm. The simulation results of digitally reconstructed images are shown in Fig. 2, we can find that for the FIL, as shown in Figs. 2(a1)–(a5), the image spots are correctly reconstructed without the influence of MIRIs. In contrast, under PCL illuminations shown in Figs. 2(b1)–2(b5), 2(c1)–2(c5), and 2(d1)–2(d5), the reconstructed image deviates from the correct one and normally becomes worse with the increase of coherence. Not surprisingly, the reconstruction quality is worst under the FCL illumination, as shown in Figs. 2(e1)–2(e5). However, it should be noted that as $Z_{\rm h}=f_{\rm d}(=0.30$ m) the correct reconstruction is always achieved regardless of the spatial coherence of the light source, indicating that the optimal recording condition of SIDH is letting the recording distance equal to the focal length of the diffractive lens loaded on the SLM. Moreover, the reconstructed image location implied by Eq. (12) is confirmed by the simulations. For example, when $Z_{\rm h}=0.15$ m, the transverse magnification is $|M_{\rm T}|=Z_{\rm h}/f_0=1.25$ according to Eq. (12), and the spacing of two SIRIs and that of two MIRIs must be 400.0 μm and 1200.0 μm, respectively, which are validated by Figs. 2(a2) and 2(e2).

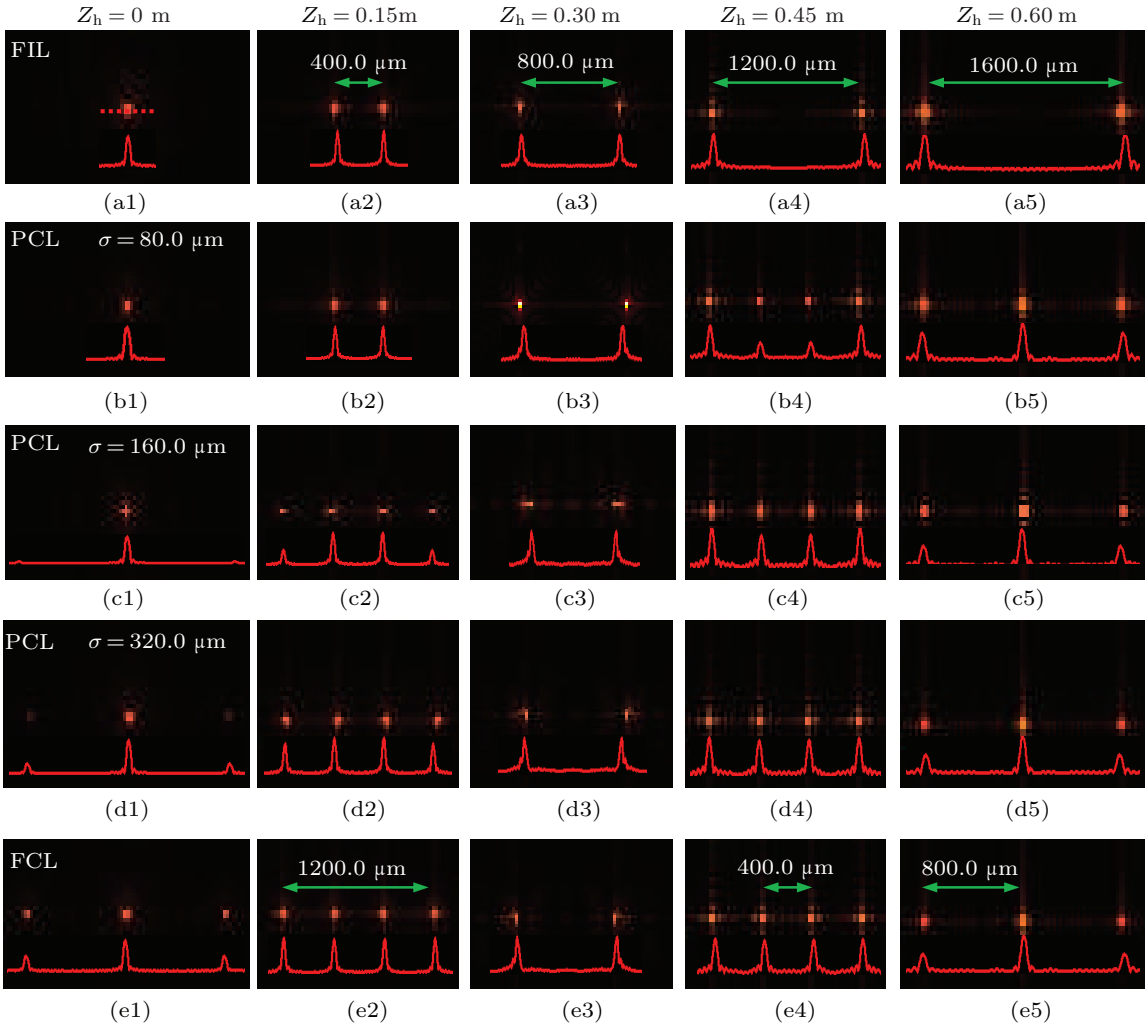


Fig. 2. Numerical results obtained by the double-point object, which is illuminated by FIL, FCL, and PCL (with $\sigma = 80.0$, 160.0, and 320 μm), respectively. The spacing of two object points is set to be 320.0 μm while keeping $f_d = 0.30$ m. The one-dimensional (1D) graphs below the spots represent the normalized intensity of the digitally reconstructed images.

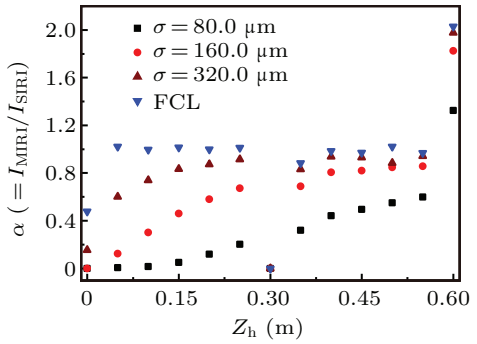


Fig. 3. Dependences of α $(= I_{MIRI}/I_{SIRI})$ on the Z_h under the illumination of FCL and PCL ($\sigma = 80.0$, 160.0, and 320.0 μm) by keeping f_d=0.30 m.

To better visualize the influence of spatial coherence on the reconstruction quality, we plot in Fig. 3 the strength ratio of the MIRI and SIRI α $(= I_{MIRI}/I_{SIRI})$ with different coherence degrees. It shows that α gradually becomes larger with the increase of Z_h, except for Z_h=f_d where MIRI vanishes. As Z_h=2f_d, due to overlapping effect of two MIRIs, the intensity of the MIRI suppresses that of the SIRI, which means that the reconstruction quality is severely deteriorated due to the MIRIs. Furthermore, figure 4 shows the simulation result for a multi-point object, the pattern of Chinese character "田" with a size of 320 μm in the x (or y) dimension. It is seen again that the quality of reconstructed image is downgraded with the increase of the spatial coherence of light. Evidently, the images have the best quality as $Z_h = f_d = 0.30$ m.

As a whole, the numerical simulation agrees well with the theoretical analysis presented in the last section and reveals a fact that the increase of the spatial coherence of illumination light will be detriment to the imaging quality of SIDH, and the impact extent of the spatial coherence depends on the recording distance of hologram. It is also worth mentioning that the above-mentioned results are akin to a previous report that investigated the influence of spatial coherence on two counter-accelerating partially coherent Airy beams;[31] with the increasing of the spatial coherence, side-lobes (*i.e.* mutual-interference spots) gradually appear and the oscillation between two main lobes becomes conspicuous.

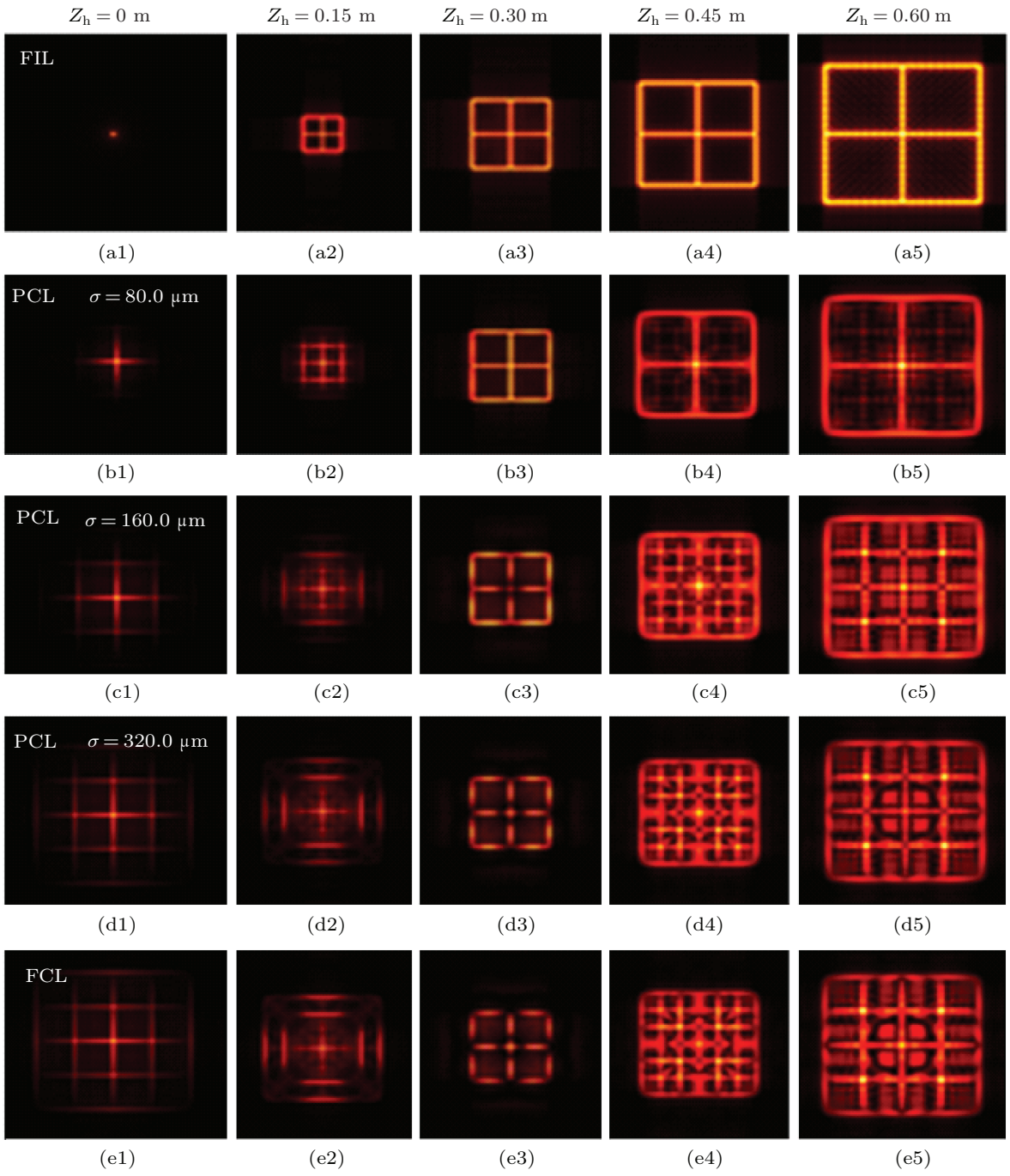


Fig. 4. Results of numerical investigation are from simulating the pattern of "⊞" which is illuminated by the FIL, FCL, and PCL, respectively.

3.2. Results of optical experiment and discussion

We carry out the optical experiments to demonstrate the impact of the spatial coherence of optical field on the image quality of SIDH. The experimental setup of our established SIDH is shown schematically in Fig. 5. The rectangle marked with solid lines shows the setup for generating the PCL, in which a fast rotating ground glass disk (RGGD) is illuminated by a focused He–Ne laser light ($\lambda = 632.8$ nm) after the lens L_1, and the RGGD is also located at the front focal plane of the lens L_2. The light beam after L_2 can be considered as the GSM beam, whose spatial coherence is determined by the size of light spot incident on the RGGD, and thus is adjusted by changing the distance l of the lens L_1 away from the RGGD. By contrast, removing the RGGD enables a fully coherent illumination.

The prepared light illuminates a test object that is placed at the front focal plane of a lens with focal length $f_0 = 0.12$ m. The object wave is lineally polarized after the polarizer P_1 whose transmission axis is oriented at a angle of 50° with respect to the active axis of a reflective phase-only SLM (Holoeye PLUTO, 1920×1080 pixels with 8.0-μm pixel pitch).

Hence, the polarized light incident upon SLM has two polarization components, one parallel and the other orthogonal to the active axis of SLM. Three diffractive lenses ($f_d = 0.30$ m) with different phase shifts ($\theta_1 = 0$, $\theta_2 = 2\pi/3$, and $\theta_3 = 4\pi/3$) sequentially written on the SLM split the incident plane waves into the signal and reference waves. After passing through the polarizer P_2, the two waves generate an interference pattern in the sensor area of a CCD camera (Pike F-505, 2452×2054 pixels with 3.45-μm pixel pitch), thus forming a digital hologram. Accordingly, three holograms are sequentially recorded on a CCD camera. The position of the CCD can be successively changed by a stepper-motor-driven long travel stage (Thorlabs, LTS300) to alter the recording distance Z_h. Due to the presence of the polarizer P_2 and the beam splitter, the recording distance Z_h is changed from 0.15 m to 0.60 m with a 0.05-m increment. Three holograms recorded by CCD are superposed according to three-step phase shifting to extract a complex amplitude responsible for the object, which is then numerically reconstructed by the computer.

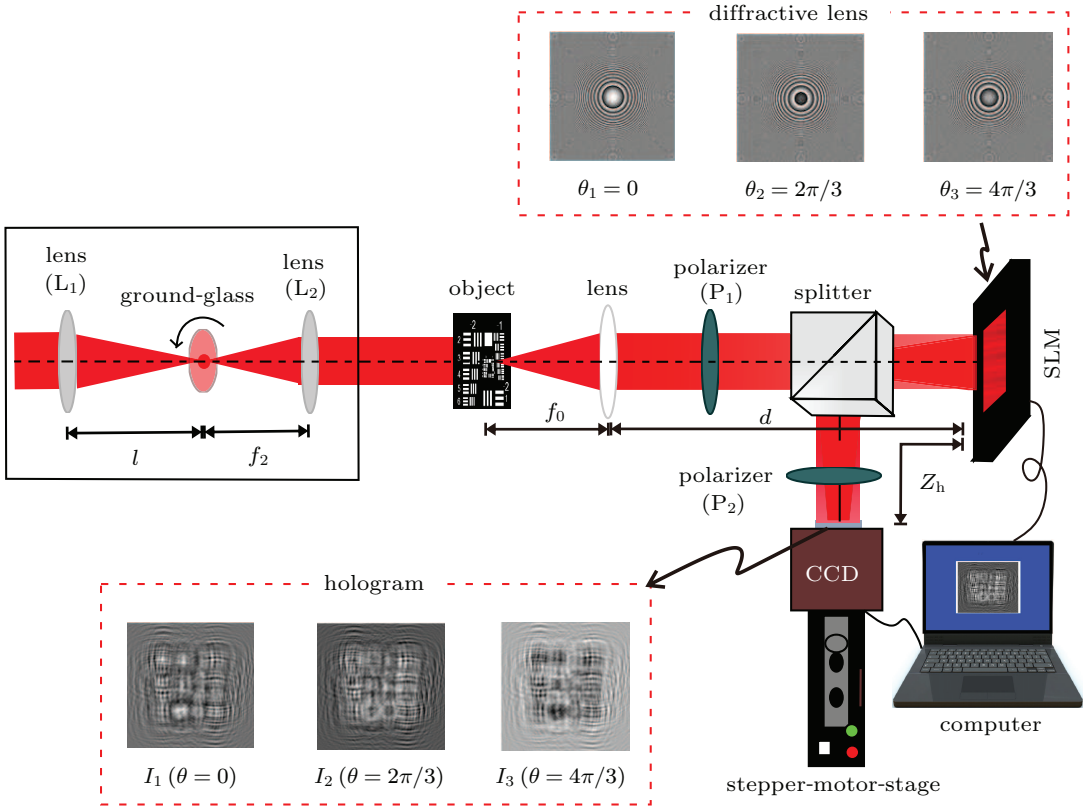


Fig. 5. Schematic representation of experimental set-up of SIDH with different spatially coherent illuminations.

The first experiment is performed for a double-hole object that has a spacing of 120.0 μm between two 50.0-μm-diameter holes. For comparisons, the object is illuminated by light with adjustable spatial coherence, and the digital hologram is recorded at four recording positions (*viz.* $Z_h = 0.15$, 0.30, 0.45, and 0.60 m). The coherence of partially coherent light (PCL) is controlled by the size of light spot incident on the RGGD; the diameter D of the spots on the RGGD is set to be 0.8, 4.0, and 8.0 mm in our experiment. According to the van Cittert–Zernike theorem of optical coherence theory,[24] for a uniformly bright incoherent source having a disc shape with a diameter D, the spatial coherence width of its radiation field at a distance z from the source is $\sigma = (\lambda z)/D$, and thus the larger diameter D of the disk spot on the RGGD means the lower spatial coherence. A fully coherent light (FCL) is provided if the RGGD is removed. The reconstructed images of the double-hole object are shown in Fig. 6. It can be found that the experimental results agree well with our theoretical analysis. For example, according to Eq. (11), as $Z_h = 0.15$ m, the theoretical values of distance between two SIRIs and between two MIRIs are 150.0 μm and 450.0 μm, respectively, and the corresponding experimental data are 155.3 μm and 458.9 μm respectively, as shown in Figs. 6(a1) and 6(d1), and thus relative measurement errors turn out to be 3.53% and 1.98%, respectively. Figure 7 shows the dependence of the ratio α ($= I_{MIRI}/I_{SIRI}$) on Z_h, and it can be found that α becomes larger with increasing Z_h under the same spatial coherence illumination. Moreover, α reaches its maximum value as $Z_h = 2f_d$.

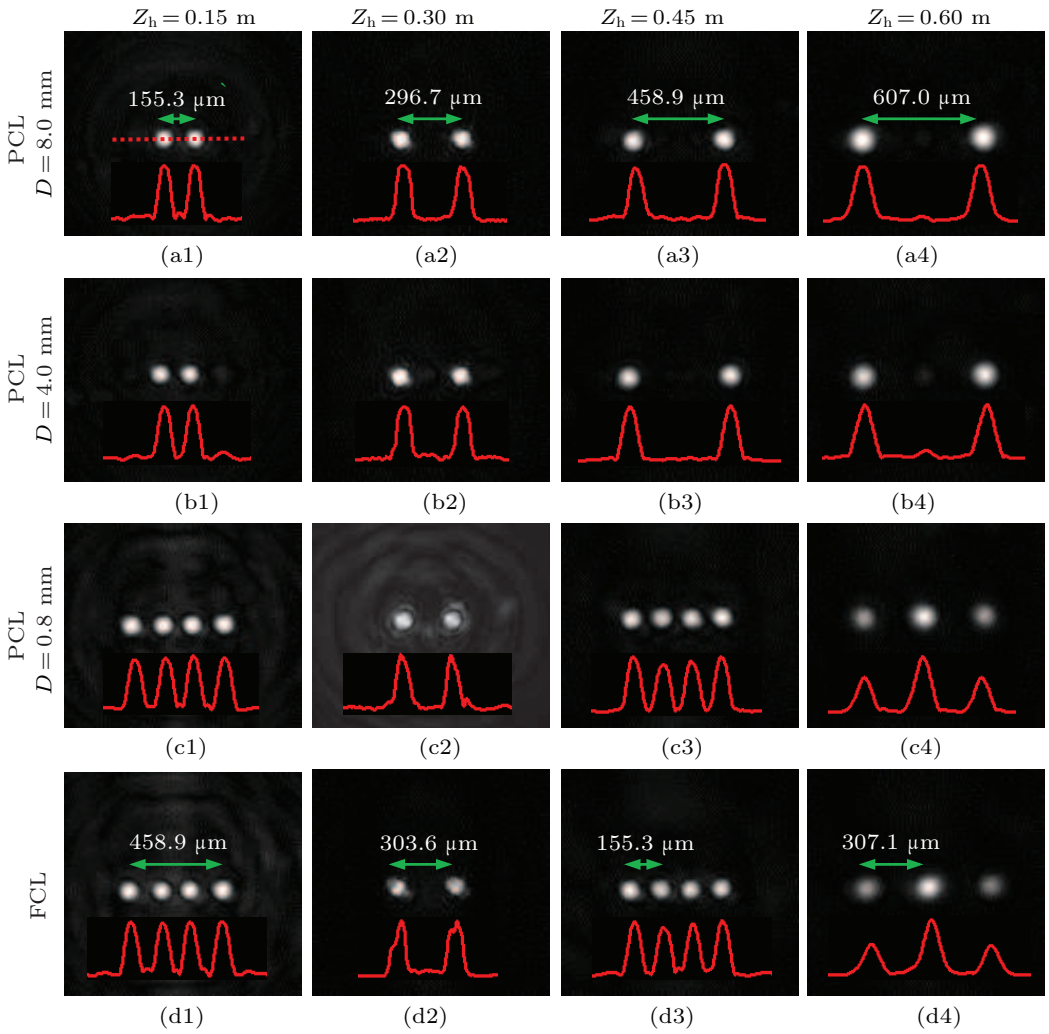


Fig. 6. Reconstructed images (bright spots) of double-hole object for different recording distance Z_h while keeping $f_d = 0.30$ m and using four light sources: the FCL (without RGGD) and the PCL produced from different light spots with the diameter D (= 0.8, 4.0, and 8.0 mm) on the RGGD. The 1D red graph below the bright spots represents the intensity profile along the line connecting two spots.

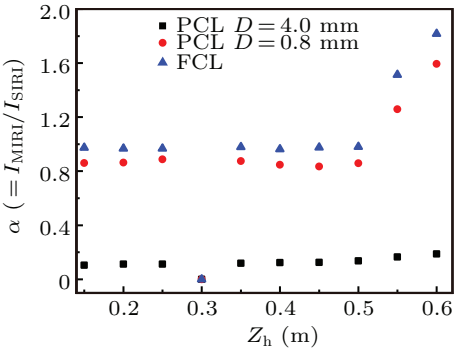


Fig. 7. The dependence of α ($= I_{MIRI}/I_{SIRI}$) on the Z_h, corresponding to Fig. 6.

The second experiment is performed for a test chart (Negative USAF1951). The experimental results are shown in Fig. 8. In order to better visualize and compare the quality of reconstructed images for different recoding distances, the size of all the images have been rescaled to be the same. The visual inspection of the experimental results provides the direct evidence that reducing the spatial coherence of illumination light (*i.e.*, enlarging D) can improve the resolution of reconstructed images. Notably, as $Z_h = f_d = 0.30$ m, the reconstructed images have the optimal resolution under the same illumination. For the purpose of comparison, we chose the element 1 of group number 4 of the USAF1951 chart as the target image region, which represents a resolution of 16 line pairs/mm and is marked with red boxes shown in Figs. 8(a1)–8(a4). The image resolution is evaluated through the visibility of the vertical lines in this target image region. We define the visibility as

$$V = (I_{max} - I_{min})/(I_{max} + I_{min}),$$

with I_{max} and I_{min} denoting the maximal and minimal intensities in the intensity profile. Figure 9(a) shows the visibility of reconstructed images with the illumination of PCL (RGGD, $D = 8.0$ mm) at different Z_h. Figure 9(b) plots the normalized intensity profile along the direction crossing the lines in the red boxes, which confirms again that the SIDH carried out when $Z_h = f_d$ (= 0.30 m) can yield an optimal reconstruction.

We should point out that letting $Z_h = f_d$ in the SIDH (*cf*. Fig. 1) implies that the CCD camera locates at the image plane of diffractive lens written on SLM. In this situation, the hologram recorded by CCD actually resembles an optical image-plane hologram, in which the requirement on spatial coherence can be the minimum.[32] Therefore, when using partially coherent light for producing an SIDH, the arrangement of image-plane hologram recording is a good choice to achieve the optimal reconstruction quality, and benefits by doing so are not only reducing the requirements on spatial coherence of the illumination light but also eliminating the influences of the MIRIs.

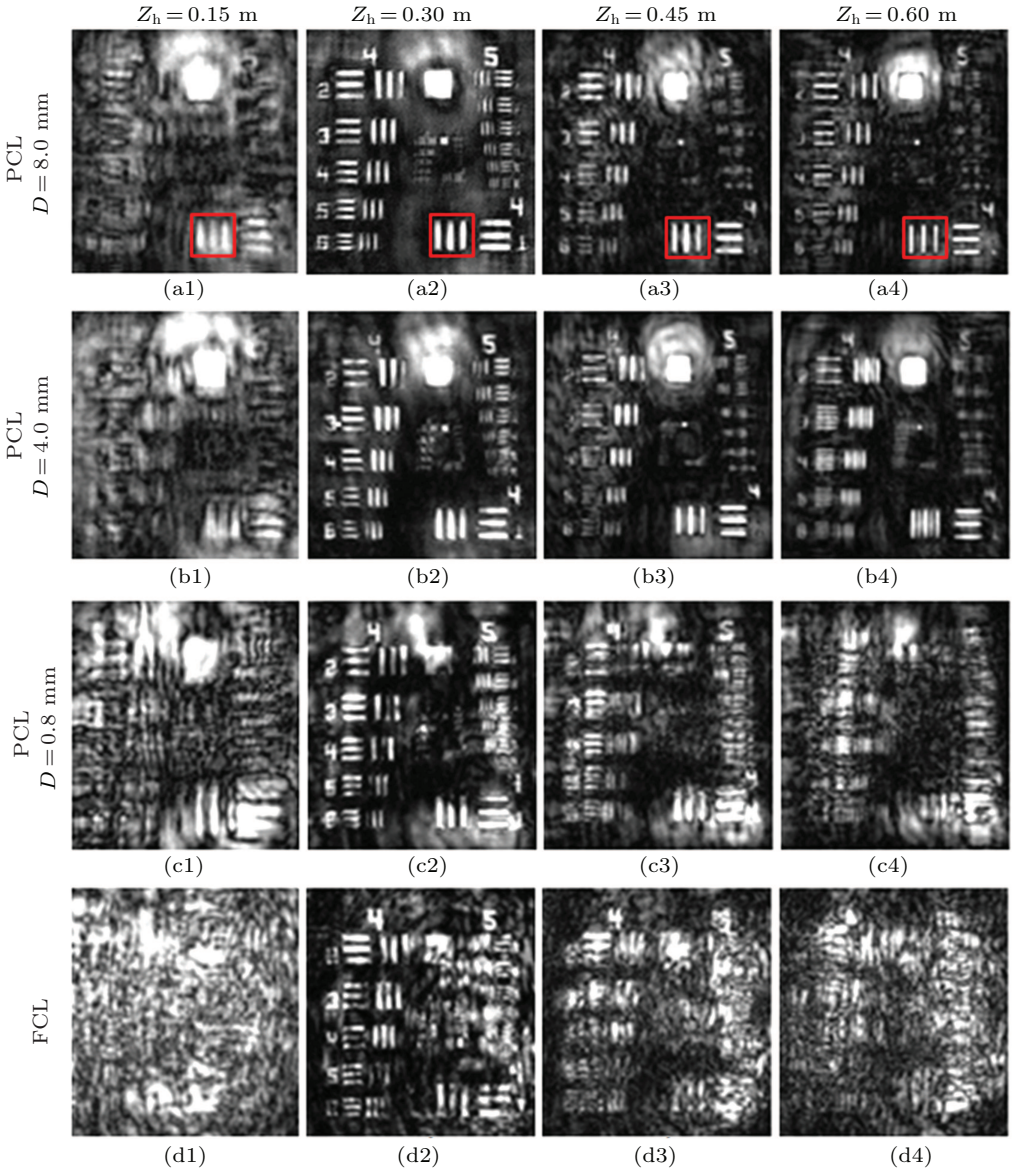


Fig. 8. Reconstructed images of test chart by keeping f_d=0.3 m, which are generated under illumination conditions analogous to those in Fig. 6.

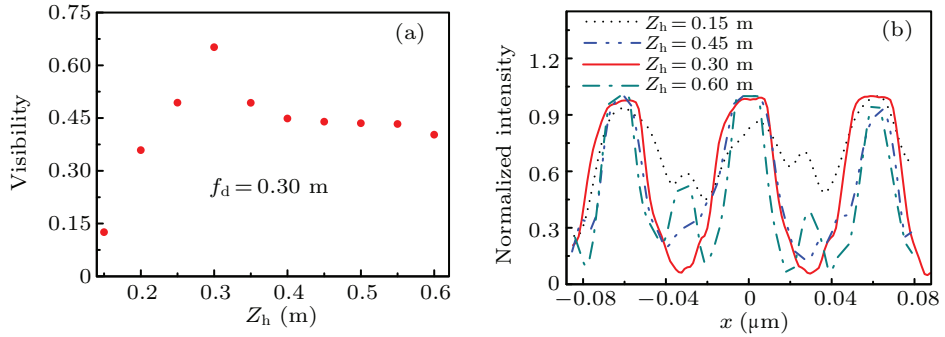


Fig. 9. (a) The dependence of visibility data of the lines marked with red rectangle in Fig. 8 on different Z_h (= 0.15, 0.30, 0.45, and 0.60 m, respectively) for the PCL illumination of $D = 8.0$ mm), (b) normalized intensity profiles crossing the corresponding line.

4. Conclusions

In summary, a remarkable aspect of the SIDH is that under the spatially incoherent light illumination it is free from speckle noises and cross-correlation image and thus yields high-quality optical reconstruction. However, the spatially incoherent light is an ideal and extreme case, and a practical light is more or less partially coherent. Thus, in many practical applications of SIDH, it would be desirable to reduce or eliminate the adverse effects of cross-correlation image resulting from spatial coherence. In this paper, based on the theory of statistical optics, we analyzed the impact of the spatial coherence on the reconstruction quality of SIDH. We validated that the spatial coherence of light beams can greatly influence the imaging characteristics of SIDH and the impact extent of the spatial coherence depends on the recording distance $Z_{\rm h}$. The findings reported here is helpful for deepening the understanding and allowing a greater exploration of SIDH, and will facilitate its applications in many fields such as phase imaging and digital microscopy.

Appendix A: Derivations of analytic expressions in Section 2

We derive the analytic expression of the complex amplitudes of the reference and signal waves arriving at the CCD plane, $U_{O_m}(\boldsymbol{C})$ and $U_{R_m}(\boldsymbol{C})$ in Eq. (7), based on the method of stationary phase.[26] Referring to Fig. 1, the signal wave impinging the CCD can be regarded as a wave diffracted from the SLM illuminated by a convergent wave. To simplify discussion, we assume that the aperture of the collimating lens is large enough, which is the case of actual experimental arrangement, so that the complex amplitude of signal wave within the CCD window can be expressed by

$$U_{O_m}(\boldsymbol{C}) = P_{\rm C}(x_{\rm C}, y_{\rm C}) \iint P_{\rm S}(x_{S_m}, y_{S_m}) \times \exp\left[{\rm i}kG^o(x_{S_m}, y_{S_m})\right] {\rm d}x_{S_m}\,{\rm d}y_{S_m}, \tag{A1}$$

where $P_{\rm C}(\boldsymbol{C})$ and $P_{\rm S}(\boldsymbol{S})$ denote the pupil function of CCD and SLM, respectively. Note that, in Eq. (A1), any multiplicative factors independent of the coordinates of (x_P, y_P), $(x_{\rm S}, y_{\rm S})$, and $(x_{\rm C}, y_{\rm C})$ are omitted for brevity, and thus $G^o(x_{S_m}, y_{S_m})$ is given by ($cf.$ Eq. (3))

$$G^o(x_{S_m}, y_{S_m}) = \frac{(x_{S_m}-x_{\rm C})^2+(y_{S_m}-y_{\rm C})^2}{2Z_{\rm h}} + \frac{(x_{P_m}^2+y_{P_m}^2)}{2f_0} - \frac{d(x_{P_m}^2+y_{P_m}^2)}{2f_0^2} - \frac{(x_{S_m}^2+y_{S_m}^2)}{2f_{\rm d}} - \frac{(x_{P_m}x_{S_m}+y_{P_m}y_{S_m})}{f_0}. \tag{A2}$$

According to the principle of stationary phase, the asymptotic approximation to the integral of Eq. (A1) is given by

$$U_{O_m}(\boldsymbol{C}) \approx P_{\rm C}(x_{\rm C}, y_{\rm C}) P_{\rm S}(x'_{S_m}, y'_{S_m}) \times \exp\left[{\rm i}kG^o(x'_{S_m}, y'_{S_m})\right], \tag{A3}$$

where the stationary points (x'_{S_m}, y'_{S_m}) are determined by

$$\left.\frac{\partial G^o(x_{S_m}, y_{S_m})}{\partial x_{S_m}}\right|_{x'_{S_m}, y'_{S_m}} = \left.\frac{\partial G^o(x_{S_m}, y_{S_m})}{\partial y_{S_m}}\right|_{x'_{S_m}, y'_{S_m}} = 0. \tag{A4}$$

By substituting Eq. (A2) into Eq. (A4) we get

$$\begin{cases} x'_{S_m} = \left(\dfrac{x_{\rm C}}{Z_{\rm h}} + \dfrac{x_{P_m}}{f_0}\right)\left(\dfrac{f_{\rm d}Z_{\rm h}}{f_{\rm d}-Z_{\rm h}}\right), \\ y'_{S_m} = \left(\dfrac{y_{\rm C}}{Z_{\rm h}} + \dfrac{y_{P_m}}{f_0}\right)\left(\dfrac{f_{\rm d}Z_{\rm h}}{f_{\rm d}-Z_{\rm h}}\right). \end{cases} \tag{A5}$$

Substituting Eq. (A5) into Eq. (A3), it follows that the phase distribution of diffracted signal wave within the CCD window, $i.e.$, $\varphi_{O_m}(\boldsymbol{C}) = kG^o(x'_{S_m}, y'_{S_m})$, is expressed by

$$\varphi_{O_m}(\boldsymbol{C}) = \frac{kf_{\rm d}Z_{\rm h}}{2(Z_{\rm h}-f_{\rm d})}\left[\frac{x_{P_m}^2+y_{P_m}^2}{f_0^2} + \frac{x_{\rm C}^2+y_{\rm C}^2}{Z_{\rm h}^2} + \frac{2x_{P_m}x_{\rm C}+2y_{P_m}y_{\rm C}}{Z_{\rm h}f_0}\right] + \frac{k\left(x_{\rm C}^2+y_{\rm C}^2\right)}{2Z_{\rm h}} + \frac{k\left(x_{P_m}^2+y_{P_m}^2\right)}{2f_0} - \frac{dk\left(x_{P_m}^2+y_{P_m}^2\right)}{2f_0^2}. \tag{A6}$$

Derivations analogous to the foregoing give the phase distribution of diffracted reference wave within the CCD window as

$$\varphi_{R_m}(\boldsymbol{C}) = k\left[-\frac{(x_{\rm C}x_{P_m}+y_{\rm C}y_{P_m})}{f_0} - \frac{Z_{\rm h}\left(x_{P_m}^2+y_{P_m}^2\right)}{2f_0^2}\right] + \frac{k\left(x_{P_m}^2+y_{P_m}^2\right)}{2f_0} - \frac{{\rm d}k\left(x_{P_m}^2+y_{P_m}^2\right)}{2f_0^2}. \tag{A7}$$

References

[1] Osten W, Faridian A, Gao P, Körner K, Naik D, Pedrini G, Singh A K, Takeda M and Wilke M 2014 *Appl. Opt.* **53** G44
[2] Kreis T 2016 *IEEE Trans. Ind. Informat.* **12** 240
[3] Kelner R and Rosen J 2015 *IEEE Trans. Ind. Informat.* **12** 220
[4] Gao H Y, Yao Q X, Pan L, Zheng Z Q, Liu J C, Zheng H D, Zeng C, Yu Y J, Sun T and Zeng Z X 2016 *Chin. Phys. B* **25** 094203
[5] Hong J and Kim M K 2013 *J. Europ. Opt. Soc. Rap. Public.* **8** 13077
[6] Kihong C, Junkyu Y, Seunghwi Y and Sung-Wook M 2017 *Opt. Lett.* **42** 3940
[7] Rosen J, Anand V, Kumar M, Ratnam M and Mukherjee S 2019 *Adv. Opt. Photon.* **11** 1
[8] Kim and Myung K 2013 *Opt. Express* **21** 9636
[9] Rosen J and Brooker G 2008 *Nat. Photon.* **2** 190
[10] Yanagawa T, Abe R and Hayasaki Y 2015 *Opt. Lett.* **40** 3312
[11] Siegel N, Lupashin V, Storrie B and Brooker G 2016 *Nat. Photon.* **10** 802
[12] Man T, Wan Y, Wu F and Wang D 2017 *Appl. Opt.* **56** F91
[13] Kim M K 2013 *Appl. Opt.* **52** A117
[14] Man T L, Wan Y H, Yan W J, Wang X H, Peterman E J G and Wang D Y 2018 *Biomed. Opt. Express* **9** 2614

[15] Katz O, Heidmann P, Fink M and Gigan S 2014 *Nat. Photon.* **8** 784
[16] Nick A, Grace K, Reinhard H, Ben M, Emrah B, Ren N and Laura W 2018 *Optica* **5** 1
[17] Hong J and Kim M K 2013 *Opt. Lett.* **38** 5196
[18] Liang D, Zhang Q, Wang J and Liu J 2020 *J. Mod. Opt.* **67** 92
[19] Weng J W, Clark D C and Kim M K 2016 *Opt. Commun.* **366** 88
[20] Tang M Y, Wu M T, Zang R H, Rong T D, Du Y L, Ma F Y, Duan Z Y and Gong Q X 2019 *Acta Phys. Sin.* **68** 104204 (in Chinese)
[21] Bouchal P, Kapitán J, Chmelík R and Bouchal Z 2011 *Opt. Express* **19** 15603
[22] Wan Y H, Man T L, Chen H, Jiang Z Q and Wang D Y 2014 *Chin. Phys. Lett.* **31** 44203
[23] Chao X B, Pan L P, Wang Z S, Yang F T and Ding J P 2019 *Acta Phys. Sin.* **68** 064203 (in Chinese)
[24] Goodman J W 2015 *Statistical optics*, 2nd edn. (John Wiley & Sons) pp. 152–219
[25] Liang M D, Chen L, Hu Y H, Lin W T and Chen Y H 2018 *Chin. Phys. B* **27** 104202
[26] Mandel L and Wolf E 1995 *Optical coherence and quantum optics* (Cambridge University Press) pp. 128–141, p. 189
[27] Xia X Y and Xia J 2016 *Chin. Phys. B* **25** 094204
[28] Rosen J and Brooker G 2007 *Opt. Lett.* **32** 912
[29] Wang F, Liu X and Cai Y 2015 *Prog. Electromagn. Res.* **150** 123
[30] Guo C S, Xie Y Y and Sha B 2014 *Opt. Lett.* **39** 2338
[31] Pang Z H and Zhao D M 2019 *Opt. Lett.* **44** 4889
[32] Sun P C and Leith E N 1994 *Appl. Opt.* **33** 597